Confinement-Induced Diffusive Sound Transport in Nanoscale Fluidic Channels

Hannes Holey,[1,2,*] Peter Gumbsch,[1,3] and Lars Pastewka[2,4,†]

[1]Institute for Applied Materials, Karlsruhe Institute of Technology, Straße am Forum 7, 76131 Karlsruhe, Germany
[2]Department of Microsystems Engineering (IMTEK), University of Freiburg, Georges-Köhler-Allee 103, 79110 Freiburg, Germany
[3]Fraunhofer Institute for Mechanics of Materials IWM, Wöhlerstraße 11, 79108 Freiburg, Germany
[4]Cluster of Excellence livMatS, Freiburg Center for Interactive Materials and Bioinspired Technologies, University of Freiburg, Georges-Köhler-Allee 105, 79110 Freiburg, Germany

(Received 5 January 2023; accepted 18 July 2023; published 21 August 2023)

Molecular dynamics (MD) simulations have been widely used to study flow at molecular scales. Most of this work is devoted to study the departure from continuum fluid mechanics as the confining dimension decreases. Here, we present MD results under conditions where hydrodynamic descriptions typically apply, but focus on the influence of in-plane wavelengths. Probing the long wavelength limit in thermodynamic equilibrium, we observed anomalous relaxation of the density and longitudinal momentum fluctuations. The limiting behavior can be described by an effective continuum theory that describes a transition to overdamped sound relaxation for compressible fluids.

DOI: 10.1103/PhysRevLett.131.084001

Nanofluidic systems have recently gained increased attention due to progress in fabrication processes [1–3], that allow exploration of the sub-nanometer confinement regime. While continuum theories have been proven robust down to the nanometer scale [4], the discrete nature of particles and even the electronic structure of the confining walls cannot be neglected at smaller scales [5,6]. The effect of the confining dimension and fluid-wall interaction has been of primary interest in numerous equilibrium [7–10] or nonequilibrium molecular dynamics (MD) simulations [11–13].

Past MD simulations of confined fluids have used simulation setups, in which the lateral box size is on the same order as the gap height. Conversely, continuum theories (such as the Reynolds equation [14]) often assume that the gap height is small compared to the lateral size. This assumption is then used to reduce the dimensionality of the governing equations by averaging over the gap, but it is clearly violated in most MD studies.

Here, we report equilibrium MD simulations that explicitly probe the long wavelength behavior of confined simple fluids. We compare the spectral behavior of transport coefficients in confined fluids to equivalent bulk systems, and derive explicit expressions for them by means of an effective continuum theory. In contrast to bulk fluids, the propagation of sound modes becomes wavelength dependent, leading to a critical transition to overdamped sound relaxation at wavelengths which scale with the square of the effective gap height. We show how to describe this overdamped, diffusive sound regime in a continuum formulation.

In our molecular simulations, fluid atoms of mass m interact through a Lennard-Jones (LJ) potential, $U(r_{ij}) = 4\epsilon[(\sigma/r_{ij})^{12} - (\sigma/r_{ij})^{6}]$, where $r_{ij} = |\vec{r}_i - \vec{r}_j|$ is the pairwise atomic distance. We use a shifted potential [15], where the shift in energy is given by the interaction energy at the cutoff radius $r_c = 2.5\sigma$. The simulations are performed both in a supercritical and a liquid state. The walls consist of two rigid layers of fcc atoms with lattice constant $a = 1.2\sigma$, where the $\{111\}$ plane is in contact with the fluid. Fluid-wall interactions are likewise modeled using a LJ potential with parameters $\sigma_{wf} = 0.875\sigma$ and $\epsilon_{wf} = 1.5\epsilon$. All simulations are in the microcanonical ensemble.

We explicitly probe the long wavelength limit of density and momentum relaxations through a simulation box with

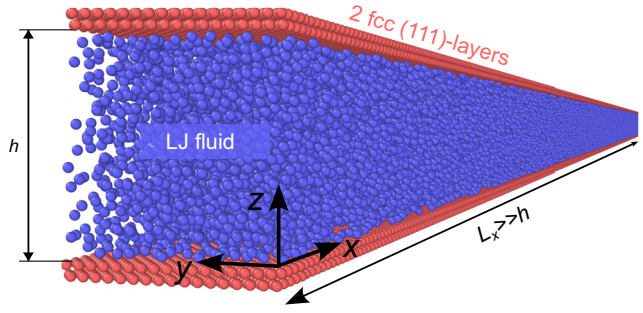

FIG. 1. Molecular dynamics simulation setup of a Lennard-Jones fluid confined between rigid walls. One of the lateral dimensions of the system is much larger than the gap height.

extreme aspect ratios, i.e., where one lateral dimension is much larger than the gap height. An exemplary setup is shown in Fig. 1. The gap height h and the box size in the y direction are 14.7σ, and the largest system is approximately 100 times longer with $L_x = 1410.9\sigma$.

Fluctuations of the collective density variables (mass and momentum) with wave vectors $\vec{k}$ are extracted using a discrete spatial Fourier transform, e.g., for mass density $\rho(\vec{k},t) = mV^{-1}\sum_{i=1}^{N}\exp(-\mathrm{i}\vec{k}\cdot\vec{r}_i(t))$, where V is the overall volume of the system. Here, we chose $\vec{k}$ parallel to the x direction and compute the normalized autocorrelation function $C_\rho(k,t) = \langle\rho^*(k,0)\rho(k,t)\rangle/\langle|\rho(k,0)|^2\rangle$ at individual wave numbers $k = |\vec{k}|$, where angular brackets denote an average over initial conditions, and the star is the complex conjugate. Similarly, we compute the autocorrelation functions of momentum density $\vec{j}$ in longitudinal ($j_\parallel = \vec{j}\cdot\hat{\vec{k}}$) and transverse direction ($\vec{j}_\perp = \vec{j} - j_\parallel\hat{\vec{k}}$), with $\hat{\vec{k}} = \vec{k}/|\vec{k}|$. In practice, we calculated the autocorrelation functions from a single long trajectory.

Figure 2 shows the normalized time autocorrelation functions of the three largest wavelengths for mass density $C_\rho(k,t)$ and longitudinal momentum density $C_\parallel(k,t)$ in a supercritical state with $T = 2.0\epsilon/k_\mathrm{B}$ and $\rho = 0.452m/\sigma^3$. In both cases, oscillations in the autocorrelation function are absent, which are usually observed in bulk systems as a signature of propagating acoustic modes due to pressure fluctuations at constant entropy. The long time behavior of the density autocorrelation in bulk fluids is shown as a dotted line in the inset of Fig. 2 for comparison. Density correlations additionally contain a purely diffusive mode arising

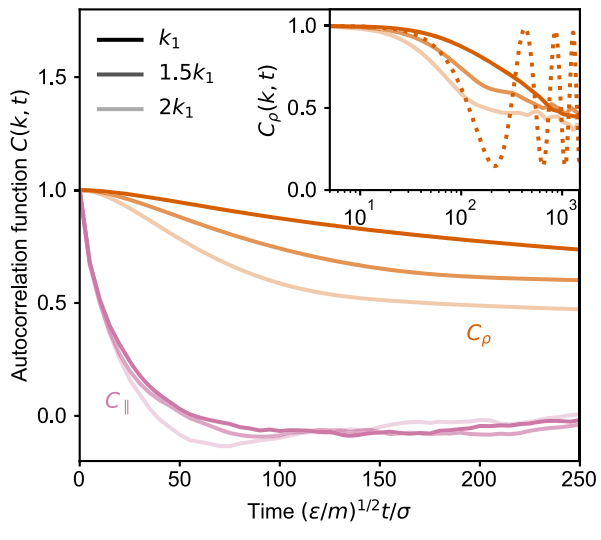

FIG. 2. Autocorrelation functions of density and longitudinal momentum fluctuations in a supercritical fluid for three modes, with the largest wavelength corresponding to $k_1\sigma = 4.45\times10^{-3}$. The inset shows the long-time behavior of density correlations on a logarithmic axis as well as the theoretical expression for the k_1 mode of an equivalent bulk fluid (dotted line).

from entropy fluctuations at constant pressure, a. k. a. the Rayleigh process describing thermal transport. Here, momentum perturbations decay rapidly, and the characteristic decay time does not show a strong dependence on longitudinal wavelength. In contrast, the decay time of the mass density autocorrelation functions depends on wavelength.

Diffusive processes in bulk systems typically yield decay rates that scale with the square of the wave number, where the constant of proportionality is the corresponding diffusivity, e.g., the kinematic viscosity $\nu = \eta/\rho$ for shear modes, or the sound absorption coefficient $\Gamma = (\gamma-1)D_\mathrm{T}/2 + \nu_\mathrm{L}/2$ for sound modes, containing both thermal diffusivity $D_\mathrm{T} = \kappa_\mathrm{T}/c_\mathrm{P}$ and kinematic longitudinal viscosity $\nu_\mathrm{L} = (4\eta/3+\zeta)/\rho$. Here, $\gamma = c_\mathrm{P}/c_\mathrm{V}$ denotes the ratio of specific heats, κ_T is the heat conductivity, and η and ζ are shear and bulk viscosities, respectively [16]. The observed mass density relaxation times are approximately 2 orders of magnitude lower than in the bulk.

To describe the deviations from bulk behavior, we consider isothermal conditions by setting $\gamma = 1$, thereby deliberately ignoring the Rayleigh process. Thus, height-averaged mass and momentum balance equations [17] are given by

$$\frac{\partial\bar{\mathbf{q}}}{\partial t} = -\frac{\partial\bar{\mathbf{f}}_x}{\partial x} - \frac{\partial\bar{\mathbf{f}}_y}{\partial y} - \underbrace{\frac{\mathbf{f}_z|_{z=h} - \mathbf{f}_z|_{z=0}}{h}}_{=:\mathbf{s}}, \tag{1}$$

where $\bar{\mathbf{q}} \equiv \bar{\mathbf{q}}(\vec{r},t) = h^{-1}\int_0^h \mathbf{q}(\vec{r},t)dz$ is the height average of the density vector of conserved variables, here expressed though the joint vector $\mathbf{q}(\vec{r},t) = (\rho(\vec{r},t), \vec{j}(\vec{r},t))^\top$, with $\vec{j} = (j_x, j_y)^\top$. Thus, the momentum component in the z direction vanishes in the reduced system. The corresponding fluxes $\mathbf{f}_i \equiv \mathbf{f}_i(\vec{r},t)$ and their height averages $\bar{\mathbf{f}}_i$ are defined by constitutive relations, and the last term $\mathbf{s}$ accounts for additional dissipation relative to a laboratory system due to the confinement

$$\bar{\mathbf{f}}_i = \begin{pmatrix} \overline{j_i} \\ \overline{p}\delta_{xi} - \bar{\tau}_{xi} \\ \bar{p}\delta_{yi} - \bar{\tau}_{yi} \end{pmatrix}, \qquad \mathbf{s} = \frac{1}{h}\begin{pmatrix} 0 \\ \tau_{xz}|_{z=h} - \tau_{xz}|_{z=0} \\ \tau_{yz}|_{z=h} - \tau_{yz}|_{z=0} \end{pmatrix}, \tag{2}$$

where we neglect convective acceleration terms. We obtain a linearized system for a compressible Newtonian fluid with viscous stress tensor $\underline{\tau} = \eta[\nabla\vec{j} + (\nabla\vec{j})^\top] + (\zeta - 2\eta/3)(\nabla\cdot\vec{j})\underline{1}$, and a barotropic equation of state $p(\rho) = c_\mathrm{T}^2\rho$, with isothermal speed of sound c_T. Spatial Fourier transform in the x and y coordinates allows us to rewrite Eq. (1) as a system of ordinary differential equations for the coefficients $\tilde{\mathbf{q}}(k,t)$ given by

$$\frac{\mathrm{d}\tilde{\mathbf{q}}(k,t)}{\mathrm{d}t} = \mathbf{H}\cdot\tilde{\mathbf{q}}(k,t), \tag{3}$$

with the hydrodynamic matrix

$$\mathbf{H} = -\begin{bmatrix} 0 & ik & 0 \\ ic_T^2 k & \nu_L k^2 + 12\nu/(h^2\kappa) & 0 \\ 0 & 0 & \nu k^2 + 12\nu/(h^2\kappa) \end{bmatrix}, \quad (4)$$

where κ denotes a permeability factor, which accounts for deviations from the no-slip boundary condition at the top and bottom interface. In a geometry with identical top and bottom walls $\kappa = 1 + 6b/h$, with Navier [18] slip length b quantifying the velocity mismatch between the wall and the outermost fluid layer. The source term in Eq. (1) vanishes only for infinitely large slip lengths where Galilean invariance is restored and the system describes a "true" bulk two-dimensional system.

The hydrodynamic matrix $\mathbf{H}$ is diagonalized with eigenvalues $\mu_\perp = -\nu k^2 - 12\nu/h^2\kappa$ corresponding to transverse modes, and $\mu_\parallel = -\nu_L k^2/2 - 6\nu/h^2\kappa \pm i s_T k$ corresponding to longitudinal modes. The phase velocity of longitudinal modes is given by the dispersion relation $s_T(k) = \sqrt{c_T^2 - 1/(\tau_\parallel k)^2}$ shown in Fig. 3, where $\tau_\parallel = (\mathrm{Re}\mu_\parallel)^{-1}$. At small wavelengths $\lambda = 2\pi/k$, sound propagation under confinement is similar to a bulk fluid, showing no dispersion, but with increasing wavelength the negative term in the discriminant takes over. For wavelengths much larger than the gap height ($hk \ll 1$) the phase velocity is approximately

$$s_T(k) = \sqrt{c_T^2 - (6\nu/h^2\kappa k)^2}. \quad (5)$$

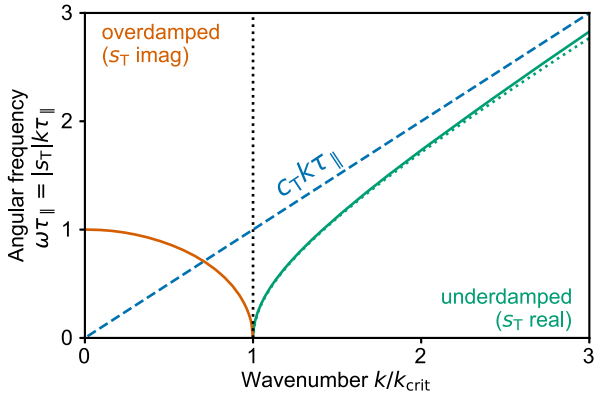

FIG. 3. Dispersion relation for a height-averaged continuum formulation of confined fluids. Solid and dotted lines describe the angular frequency using the magnitude of the phase velocity with [Eq. (5)] and without long wavelength approximation, respectively. The dashed line describes the bulk reference. The wave number is normalized by $k_{crit} = 6\nu/h^2\kappa c_T$ and the angular frequency is normalized by the characteristic relaxation time of longitudinal modes in the underdamped limit $\lim_{k\to k_{crit}} \tau_\parallel = h^2\kappa/6\nu$. The critical transition from underdamped to overdamped dynamics occurs with diverging group velocity.

Thus, longitudinal modes become critically damped at $k_{crit} = 6\nu/h^2\kappa c_T$ with diverging group velocity $d(s_T k)/dk$. Consequently, s_T is imaginary for $k < k_{crit}$ and $\mathbf{H}$ has only real eigenvalues. This leads to a bifurcation in the relaxation of sound modes, leading to the two distinct behaviors shown in Fig. 2. In this overdamped regime, one can easily show that density fluctuations decay with a rate $\propto k^2$, whereas the relaxation time of longitudinal momentum fluctuations converges ($\lim_{k\to 0}\tau_{j,\parallel} = \tau_\perp$).

The real part of the solution to Eq. (3) for arbitrary initial conditions $\tilde{\mathbf{q}}(k,0) = [\tilde{\rho}(k,0), \tilde{j}_\parallel(k,0), \tilde{j}_\perp(k,0)]^\top$ is given by

$$\frac{\tilde{\rho}(k,t)}{\tilde{\rho}(k,0)} = e^{-t/\tau_\parallel}\left[\cos(s_T k t) + \frac{1}{s_T k \tau_\parallel}\sin(s_T k t)\right], \quad (6a)$$

$$\frac{\tilde{j}_\parallel(k,t)}{\tilde{j}_\parallel(k,0)} = e^{-t/\tau_\parallel}\left[\cos(s_T k t) - \frac{1}{s_T k \tau_\parallel}\sin(s_T k t)\right], \quad (6b)$$

$$\frac{\tilde{j}_\perp(k,t)}{\tilde{j}_\perp(k,0)} = e^{-t/\tau_\perp}, \quad (6c)$$

with characteristic relaxation times

$$\tau_\perp(k) = (\nu k^2 + 12\nu/h^2\kappa)^{-1}, \quad (7a)$$

$$\tau_\parallel(k) = (\nu_L k^2/2 + 6\nu/h^2\kappa)^{-1}. \quad (7b)$$

Note, that these expressions have the same functional form as in the bulk case [16], but characteristic times describing the decay and oscillations differ. Furthermore, in the case of confined fluids, Eqs. (6) remain valid when s_T becomes purely imaginary and the trigonometric functions turn into their hyperbolic counterparts, which is not observed in the bulk.

We proceeded by testing Eqs. (6) using MD simulations of a LJ liquid with $T = 0.8\epsilon/k_B$ and $\rho = 0.845m/\sigma^3$ for a wide range of wavelengths. Figures 4(a) and 4(b) show the autocorrelation functions of longitudinal momentum fluctuations for both bulk and slab systems for $\lambda = 188.1\sigma$ and $\lambda = 470.3\sigma$, respectively. We obtain the angular frequency of the oscillations and the decay rate of the amplitude from a least-squares fit to the theoretical expressions.

Figure 4(c) plots the phase velocity over the wavelength for both bulk and confined liquids. To show the applicability of the isothermal, height-averaged continuum theory, we compute the viscosity, speed of sound and slip length in separate MD simulations and predict the phase velocity using Eq. (5). Our predictions are in good agreement with the speed of sound obtained from the fits to the autocorrelation functions as shown in Fig. 4(c). The predicted critical wavelength $\lambda_{crit} = 914.3\sigma$ is below the size of the domain and seems to slightly underestimate the MD data.

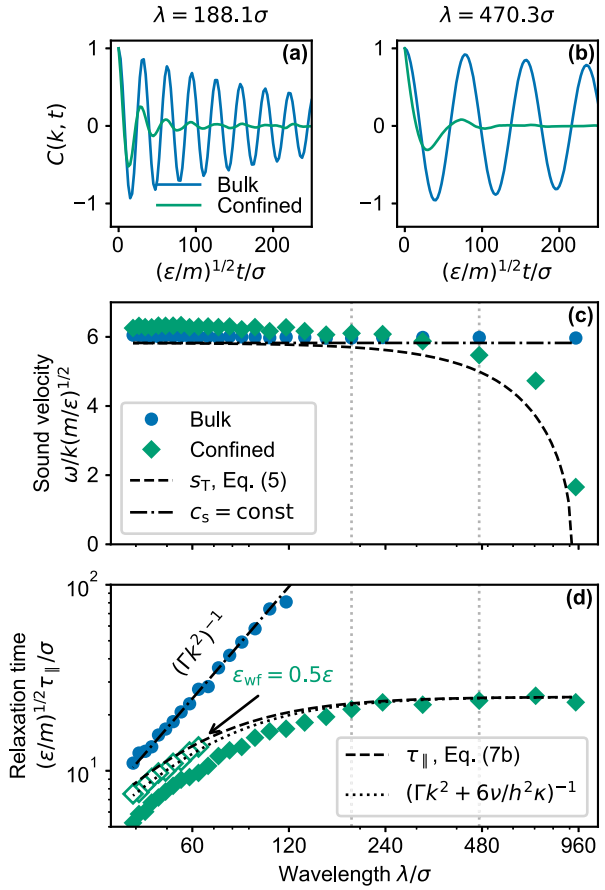

FIG. 4. Comparison of longitudinal momentum fluctuations in bulk and confined LJ liquids. Sound frequency and attenuation constants are obtained from a fit to autocorrelation functions at various wavelengths, e.g., as shown in panel (a) and (b). The sound velocities (c) and relaxation times (d) are then compared to the theoretical predictions from Eqs. (5) and (7b), respectively. Viscosity and speed of sound are computed from separate bulk equilibrium simulations, and nonequilibrium MD simulations have been performed to obtain the slip length. The continuum model describes the MD data reasonably well. Deviations between the model and the data at small wavelengths are due to effective viscosity enhancement in the confined system compared to the bulk. Lowering wall-fluid interaction energies leads to a better agreement in the low wavelength regime, as shown by the open diamonds in panel (d). Transition to overdamped behavior is expected for wavelengths larger than 914.3σ. Note that the speed of sound measured from MD is adiabatic (c_s) rather than isothermal (c_T).

Figure 4(d) plots relaxation times of longitudinal modes over the wavelength. Our prediction based on Eq. (7b) with viscosities and slip length obtained from equilibrium Green-Kubo (GK) and nonequilibrium Couette flow simulations (see Table I), respectively, agrees with the relaxation time obtained from fits to the autocorrelation functions. At small wavelengths, the prediction can be improved by considering the thermal contribution to the sound absorption naturally included in our MD setup, where we used

TABLE I. Viscosities and slip lengths of the considered LJ systems obtained from separate MD simulations.

	Liquid[a]	Supercritical[b]	Units
Shear viscosity η	3.077	0.550	$\sqrt{m\epsilon}/\sigma^2$
Bulk viscosity ζ	1.077	0.351	$\sqrt{m\epsilon}/\sigma^2$
Slip length[c] b	3.741	0.608	σ

[a] $\rho = 0.845m/\sigma^3$, $T = 0.8\epsilon/k_B$.
[b] $\rho = 0.452m/\sigma^3$, $T = 2.0\epsilon/k_B$.
[c] Couette flow, mean of runs with wall velocity $U \in [10,20]$ m/s.

thermophysical data for argon from NIST [19] to obtain the additional parameters γ and D_T. Yet, the isothermal theory captures the long-wavelength effects sufficiently well. Remaining deviations at small wavelengths are due to layering effects in the confined system with strong wall fluid interactions, which may lead to higher viscosities than in the bulk GK simulations. Lowering the interfacial interaction energy leads to quantitative agreement also at small wavelengths.

Hydrodynamic theory adequately describes the relaxation behavior of confined fluids, as shown for the liquid LJ system, but all considered wavelengths were below the transition to overdamped relaxation. Figure 5 shows the sound relaxation times for the supercritical fluid. Note that the supercritical state here and in Fig. 2 was chosen for practical purposes, since it allows probing the overdamped regime at lower computational cost than in the liquid state. For the confined system and wavelengths in the underdamped regime, Eq. (7b) describes the transition from quadratic wavelength dependence to constant relaxation times analogously to the LJ liquid described above. The expected critical transition based on bulk equilibrium and

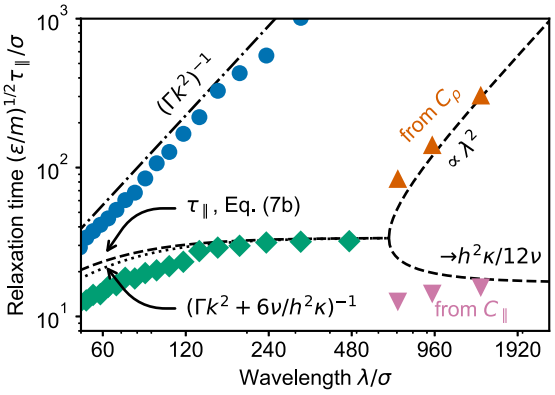

FIG. 5. Sound relaxation times obtained from fits to the autocorrelation functions of longitudinal momentum and density fluctuations in the supercritical LJ fluid. Bulk and underdamped behavior is similarly described as in Fig. 4(d), but the lower critical wavelength ($\lambda_{crit} = 689.3\sigma$) allows easier exploration of the overdamped regime. Upwards and downwards pointing triangles are fitted density and longitudinal momentum relaxation times, respectively.

Couette flow simulations occurs at $\lambda_{\mathrm{crit}} = 689.3\sigma$. Exponential decay rates from fits to both longitudinal momentum and density correlation functions beyond λ_{crit} converge towards the continuum prediction in the long wavelength limit.

The transition from underdamped to overdamped sound transport has first been addressed by Ramaswamy and Mazenko [20], who discussed the influence of friction on the dynamics of adsorbates. However, they do so without further quantification of the underlying friction term that interpolates between hydrodynamic and diffusive behavior. Later, anomalous, algebraic long-time tails of velocity autocorrelation functions of suspended particles under confinement, which were observed in lattice-Boltzmann simulations, have been explained by the same effect [21,22]. A rigorous mathematical treatment of the problem was then given by Felderhof [23]. Here, we showed that a simplified gap-averaged treatment of the fluid film accurately describes the long wavelength behavior as confirmed by our MD simulations.

The critical transition scales quadratically with an effective gap height $h\sqrt{\kappa}$. Because of this scaling relation, overdamped sound does not play a role on macroscopic length scales, but may become important when the confining dimension is reduced to microscales or nano scales, e.g., the critical wavelength of ambient water in a circular channel is approximately 230 km for a radius $R = 1$ cm, but only 230 nm at $R = 10$ nm (assuming no slip). Hence, lateral dimensions can substantially influence mass transport at small scales. Channels with lengths greater than the critical wavelength are dominated by diffusion and may show disproportionately slower mass transport than shorter channels of the same gap height. Experimental evidence of the transition to diffusive dynamics might be provided either by measuring flow characteristics in different channel geometries, or—in the spirit of the presented results on collective fluctuations—through Brillouin light scattering techniques. With increasing technological relevance of *single-digit* nanofluidic devices, the effect might play an important role in tailoring transport properties therein.

All MD simulations were performed with LAMMPS [24]. The authors gratefully acknowledge support by the German Research Foundation (DFG) through GRK 2450. Furthermore, the authors acknowledge support by the state of Baden-Württemberg through bwHPC, for calculations carried out on bwForCluster NEMO (DFG Grant No. INST 39/963-1 FUGG) and bwUniCluster2.0. Data is stored on bwSFS (University of Freiburg, DFG Grant No. INST 39/1099-1 FUGG).

*hannes.holey@kit.edu
†lars.pastewka@imtek.uni-freiburg.de

[1] J. Feng, M. Graf, K. Liu, D. Ovchinnikov, D. Dumcenco, M. Heiranian, V. Nandigana, N. R. Aluru, A. Kis, and A. Radenovic, Nature (London) **536**, 197 (2016).
[2] B. Radha, A. Esfandiar, F. C. Wang, A. P. Rooney, K. Gopinadhan, A. Keerthi, A. Mishchenko, A. Janardanan, P. Blake, L. Fumagalli, M. Lozada-Hidalgo, S. Garaj, S. J. Haigh, I. V. Grigorieva, H. A. Wu, and A. K. Geim, Nature (London) **538**, 222 (2016).
[3] R. H. Tunuguntla, R. Y. Henley, Y.-C. Yao, T. A. Pham, M. Wanunu, and A. Noy, Science **357**, 792 (2017).
[4] L. Bocquet and E. Charlaix, Chem. Soc. Rev. **39**, 1073 (2010).
[5] N. Kavokine, R. R. Netz, and L. Bocquet, Annu. Rev. Fluid Mech. **53**, 377 (2021).
[6] N. Kavokine, M.-L. Bocquet, and L. Bocquet, Nature (London) **602**, 84 (2022).
[7] L. Bocquet and J.-L. Barrat, Phys. Rev. Lett. **70**, 2726 (1993).
[8] L. Bocquet and J.-L. Barrat, Phys. Rev. E **49**, 3079 (1994).
[9] F. Porcheron and M. Schoen, Phys. Rev. E **66**, 041205 (2002).
[10] K. Huang and I. Szlufarska, Phys. Rev. E **89**, 032119 (2014).
[11] P. A. Thompson and M. O. Robbins, Phys. Rev. A **41**, 6830 (1990).
[12] N. V. Priezjev and S. M. Troian, Phys. Rev. Lett. **92**, 018302 (2004).
[13] A. Martini, H.-Y. Hsu, N. A. Patankar, and S. Lichter, Phys. Rev. Lett. **100**, 206001 (2008).
[14] D. Dowson, Int. J. Mech. Sci. **4**, 159 (1962).
[15] M. H. Müser, S. V. Sukhomlinov, and L. Pastewka, Adv. Phys.: X **8**, 2093129 (2023).
[16] J.-P. Hansen and I. R. McDonald, *Theory of Simple Liquids*, 3rd ed. (Elsevier/Academic Press, Amsterdam, Boston, 2007).
[17] H. Holey, A. Codrignani, P. Gumbsch, and L. Pastewka, Tribol. Lett. **70**, 36 (2022).
[18] C. L. M. H. Navier, Mém. L'Académie R. Sci. L'Institut Fr. **6**, 389 (1823).
[19] E. W. Lemmon, I. H. Bell, M. L. Huber, and M. O. McLinden, in *NIST Chemistry WebBook, NIST Standard Reference Database Number 69*, edited by P. J. Linstrom and W. G. Mallard (National Institute of Standards and Technology, Gaithersburg, MD, 2023).
[20] S. Ramaswamy and G. F. Mazenko, Phys. Rev. A **26**, 1735 (1982).
[21] M. H. J. Hagen, I. Pagonabarraga, C. P. Lowe, and D. Frenkel, Phys. Rev. Lett. **78**, 3785 (1997).
[22] I. Pagonabarraga, M. H. J. Hagen, C. P. Lowe, and D. Frenkel, Phys. Rev. E **58**, 7288 (1998).
[23] B. U. Felderhof, J. Chem. Phys. **124**, 054111 (2006).
[24] A. P. Thompson, H. M. Aktulga, R. Berger, D. S. Bolintineanu, W. M. Brown, P. S. Crozier, P. J. in 't Veld, A. Kohlmeyer, S. G. Moore, T. D. Nguyen, R. Shan, M. J. Stevens, J. Tranchida, C. Trott, and S. J. Plimpton, Comput. Phys. Commun. **271**, 108171 (2022).